

# Shaped-Charge Jet-Initiation of Covered RDX-Based Aluminized Explosives and Effect of Temperature

Pin Zhao,<sup>[a]</sup> Lang Chen,\*<sup>[a]</sup> Kun Yang,<sup>[a]</sup> Yiwen Xiao,<sup>[a]</sup> Kaining Zhang,<sup>[a]</sup> Jianying Lu,<sup>[a]</sup> and Junying Wu<sup>[a]</sup>

**Abstract:** Understanding the shaped-charge jet-initiation mechanism of covered explosives and the effect of explosive temperature is important for ammunition safety. We devised a method of using a shaped-charge jet-penetrating cover to shock-initiate heated explosives. This method achieves uniform temperature control of explosives via heating the upper and lower ends and preserves heat on the side of the explosive charge. We experimentally tested the method on hexahydro-1,3,5-trinitro-1,3,5-triazine (RDX)-based aluminized explosives (61 wt.% RDX, 30 wt.% Al, 9 wt.% binder) at different temperatures and cover thicknesses. The jet-penetration behavior and explosive detonation-wave growth were observed via X-ray photography, and the effect of explosive temperature on jet initiation was analyzed. A numerical model of the shaped-charge jet-initiating explosive was set up by considering the temperature change of the explosive and analyzing the detonation-wave growth and initiation thresholds of different

explosive temperatures under jet shock initiation. Under a thin cover, the explosive showed prompt impact initiation by the jet; the initiation occurred very near to the explosive surface. However, for a thick cover, the explosion was initiated by a bow wave formed at a certain distance from the upper surface of the explosive, and a retonation wave was observed. The temperature of RDX-based aluminized explosives affects the two jet-initiation mechanisms. The shock sensitivity of the explosives to the jet decreased with increasing temperature, but the shock sensitivity increased when the temperature exceeded a certain value. A simulation method was established that can be used to predict shaped-charge jet initiation at different explosive temperatures. We obtained the relationship between the cover thickness and run-to-detonation distance under jet shock initiation, which provides a theoretical basis for safety analysis and evaluation of a warhead charge that is attacked by a shaped-charge jet.

**Keywords:** Shaped-charge jet · Impact initiation · Bow-wave initiation · Cover thickness · Temperature

## 1 Introduction

Researchers who study ammunition safety are concerned about the reaction mechanism and response law of ammunition under jet attack. Under certain circumstances, an unexpected condition arises in which ammunition may be heated and penetrated by a shaped-charge jet. Therefore, it is important to investigate the effect of explosive temperature on jet initiation.

Earlier studies of shaped-charge jet-initiating explosives suggested that a high-speed jet initiated the explosive via direct impact [1, 2]. Held [3] used X-ray photography to conduct experiments on jet-initiating explosives of different diameters, and proposed that the squared jet velocity ( $V^2$ ) multiplied by the jet diameter ( $d$ ) was the critical value for jet initiation. Mader et al. [4, 5] used the forest-fire model to simulate the shock-initiation experiments conducted by Held [3]. They found that, below the critical value of  $V^2d$ , a shock wave produced by the jet tip with a certain propagation duration caused detonation in the jet-penetrating explosive. This is different from the impact mechanism based on initiation time. Chick et al. [6] used X-ray radiography to observe the run-to-detonation distance in an experiment where a curved shock-wave forward jet tip ini-

tiated an explosive under thick cover. Near the onset of detonation, a retonation was produced that moved back through the previously shocked explosive, which was expanding radially. This behavior was termed bow-wave initiation and differed from prompt impact initiation under a thin cover or without a cover. In subsequent experiments [7] and simulations [8] with bow-wave initiation, Chick et al. found that the run distance to detonation reached tens of millimeters and lasted tens of microseconds, and the simulation gave the explosive pressure distribution. Frey et al. [9] simulated jet-initiating explosives covered by a thick barrier and found that a long-distance was required to form the bow wave, which delayed initiation and increased the run distance to detonation. After summarizing the experimental results, Chick et al. [10] proposed that prompt impact initiation occurred when the ratio of the critical failure diameter ( $D$ ) to the jet diameter ( $d$ ) was below 5, and

[a] P. Zhao, L. Chen, K. Yang, Y. Xiao, K. Zhang, J. Lu, J. Wu  
State Key Laboratory of Explosion and Science  
Beijing Institute of Technology  
No.5, Zhongguancun South Street, Haidian District, Beijing, China  
Fax: +86-10-6891 8035  
\*e-mail: chenlang@bit.edu.cn

bow-wave initiation occurred if  $D/d > 5$ . Lawrence et al. [11] used the forest-fire model to simulate impact and bow-wave initiation and found that the explosive detonated promptly under subsonic and supersonic jet penetration. However, bow-wave initiation occurred only when the jet diameter was small enough and penetrated the explosive at supersonic speed. Chick et al. [12] carried out further experiments on jet penetration by varying the barrier thickness to initiate the explosive, and also found that  $D/d$  was a determining factor in bow-wave initiation. Mellor et al. [13] used the CREST burn-rate model to simulate a jet-initiating covered explosive. The simulation showed that the pressure during bow-wave initiation decayed from the jet tip to the bow wave, and there was insufficient compression before the bow wave to contribute to detonation. Explosive detonation occurred only when the bow wave propagated a certain distance in a period and reached a certain magnitude. Under critical conditions close to prompt impact initiation, a delay occurred in reaching a point where the detonation could diverge. This caused extended run distances, which is consistent with the experiments conducted by James et al. [14]. They found that cover materials [15, 16] also influenced impact and bow-wave initiation, and the jet-tip shape only affected the impact initiation [17]. These studies have focused on the jet-initiating mechanism and law at ambient temperature; however, little investigation has been conducted into jet-initiating explosives at high temperature.

The explosive shock sensitivity changes with temperature. Schwartz [18] conducted experiments with a flyer impacting on heated 1,3,5-triamino-2,4,6-trinitrobenzene (TATB)-based explosives and found that the shock sensitivity increased with increasing temperature. Urtiew et al. [19] carried out shock-initiation experiments on heated octahydro-1,3,5,7-tetranitro-1,3,5,7-tetrazocine (HMX)-based explosives and reported that the shock sensitivity improved significantly when the crystal HMX phase changed. Garcia et al. [20] found that increasing the volume of 2,6-diamino-3,5-dinitropyrazine-1-oxide (LLM-105) improved the explosive shock sensitivity. The particle velocity inside explosives was measured at different temperatures by Gustavsen et al. [21–23], who found that the detonation distance decreased with increasing temperature. Chen et al. [24] conducted experiments using explosive-driven, flyer-initiating, heated hexanitrohexaazaisowurtzitane (CL-20). The CL-20 crystal phase changed at high temperatures, which weakened the shock sensitivity. They [25] also found that a decrease in shock sensitivity was caused by binder softening during the heating of RDX-based aluminized explosive. Researchers understand the shock-initiation law of several explosives at high temperature. However, studies are lacking on the jet-initiation mechanism and law for heated explosive; hence, there is no theoretical basis for safety analysis and evaluation of heated ammunition attacked by jets.

In this study, we assembled a device in which an explosive is heated in a shaped-charge jet-penetrating cover.

The upper and lower explosive surfaces are heated, and heat preservation on the side of the explosive is used to achieve uniform temperature control. X-ray radiography was used to observe jet penetration of the cover and detonation-wave growth. A shaped-charge jet-shock-initiation experiment was carried out for RDX-based aluminized explosives at different temperatures and cover thicknesses. We also analyzed the effect of explosive temperature on jet impact and bow-wave initiation. The obtained relationship between shock sensitivity and temperature was used to establish mathematical models of impact and bow-wave initiation. The laws relating the run-to-detonation distance and initiation threshold with temperature were obtained and analyzed for both initiation mechanisms.

## 2 Jet-Initiation Experiment for Covered and Heated Explosive

Figure 1 shows the device for jet initiation of a covered and heated explosive, which consists of a detonator, a metallic liner, a shaped charge, a cover, a tested explosive, heaters, thermocouples, and an aluminum plate. The structural dimensions of the metal liner and shaped charge are shown in Figure 2. During the test, the shaped charge was placed 60 mm above the steel cover with a tested explosive charge below the steel cover and an aluminum plate on the bottom of the explosive. Heaters were placed on the upper surface of the cover and the lower surface of the aluminum plate to heat the explosive, and rock wool was wrapped on the side of the explosive to preserve heat. Thermocouples were fixed on the surfaces of the cover and aluminum plate and on the side of the explosive to measure temperature. The temperature of the heated explosive was controlled with temperature-control machines [26]. The explosive was heated initially. The explosive charges were heated to the desired temperature by a rate of 5 K/min, then kept at this temperature for a while. When the cover, aluminum plate, and explosive reached the predetermined temperature, the detonator initiated the shaped charge and a high-speed metal jet was generated to initiate the covered explosive.

The jet initiation of the covered explosive was observed via X-ray radiography, a schematic of which is shown in Figure 3. The experimental measurement system consisted of two X-ray light pipes, a protective wall, the experimental device, and negative films. Two X-rays were emitted from the side and passed through the experimental device. Images were obtained on negative films behind the experimental device. Materials of different densities showed grayscale variation on the negative films, indicating changes in explosive structure. An electrical signal was used to initiate the X-ray source and was measured with an ionization probe on the upper surface of the shaped charge. The radiograph times of the explosive were controlled with two light-emitting tubes by setting different light-emission delay times.

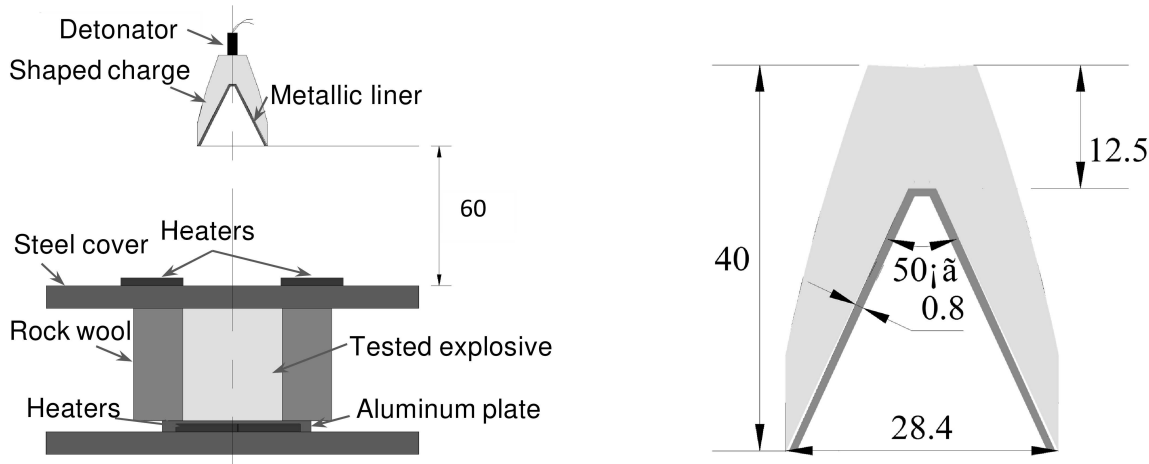


Figure 1. Device for jet initiation of covered and heated explosive.

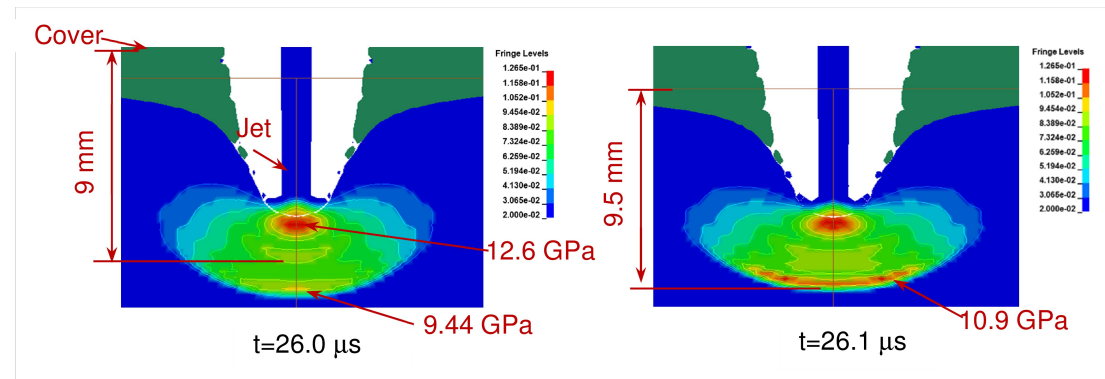


Figure 2. Structure of shaped charge and Unit: mm metallic liner. Unit: mm

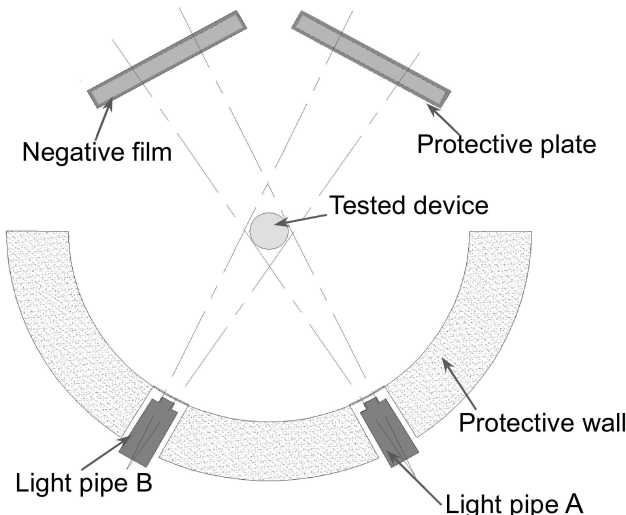


Figure 3. Schematic of X-ray radiography for jet-initiating explosive experiment.

The shaped charge was HMX-based explosive (95 wt.% HMX, 5 wt.% binder), with a charge density of  $1.8 \text{ g/cm}^3$ . The experimental explosive was RDX-based aluminized explosive with a diameter of 40 mm and a charge 50 mm long. The steel cover had a diameter of 150 mm. Jet initiation of the RDX-based aluminized explosive was performed at  $25^\circ\text{C}$  and  $75^\circ\text{C}$  for steel cover thicknesses of 2 mm and 27 mm, respectively.

### 3 Simulated Jet Initiation of Covered and Heated Explosive

Because of the limited number of experiments conducted, only jet and detonation waves with a single time were observed. It is difficult to carry out further analysis on the laws and mechanisms of jet-initiating explosives. Therefore, we simulated the detonation using nonlinear finite-element analysis [27] to determine the jet-initiation law of explosives at different temperatures.

The model considered the metal liner, shaped charge, cover, RDX-based aluminized explosive, and the surrounding air domain. A vacuum-material model was used to describe air, and an HMX-based shaped charge was described using a high-explosive model and the Jones–Wikins–Lee (JWL) equation of state for products. Table 1 shows the JWL parameters for the HMX-based explosives. The copper liner was described using the Johnson–Cook model and the Grüneisen equation of state. The elastoplastic hydrodynamic-material model and the Grüneisen equation of state were applied to the cover. Table 2 shows the material model parameters for the cover and copper liner. Initiation of the RDX-based aluminized explosive was described by the Lee–Tarver ignition-and-growth model and the JWL equation of state, which considered the temperature variation of the explosive.

The equation of the ignition-and-growth reaction rate is [28]

$$\frac{d\lambda}{dt} = I(1-\lambda)^b \left(\frac{\rho}{\rho_0} - 1 - a\right)^x + G_1(T)(1-\lambda)^c \lambda^d P^y + G_2(1-\lambda)^e \lambda^g P^z \quad (1)$$

where  $\lambda$  is the explosive reaction degree;  $t$  is the time;  $\rho$  is the density;  $\rho_0$  is the initial density;  $P$  is the pressure; and  $I$ ,  $G_1$ ,  $G_2$ ,  $a$ ,  $b$ ,  $x$ ,  $c$ ,  $d$ ,  $y$ ,  $e$ ,  $g$ , and  $z$  are constants. The first term on the right of Eq. (1) is the ignition term, and  $I$  and  $x$  determine the number of ignition hot spots. The latter two terms on the right side are the growth and completion terms, and  $G_1(T)$  and  $d$  determine the early growth of the hot spot after ignition. The parameter  $G_1(T)$  changes with increasing temperature. In the completion term,  $G_2$  and  $z$  determine the reaction rate of the explosives at high pressure.

The parameter  $G_1(T)$  is fitted as a function of temperature  $T$  for the RDX-based aluminized explosive [23]:

$$G_1(T) = \begin{cases} 453 - 1.960(T - 25) & 25^\circ\text{C} \leq T \leq 111^\circ\text{C} \\ 284 + 1.579(T - 111) & 111^\circ\text{C} < T \leq 170^\circ\text{C} \end{cases} \quad (2)$$

The unreacted and product JWL equations of state are [26]:

$$P_E = Ae^{-R_1 V_E} + Be^{-R_2 V_E} + \frac{\omega C_v T_0}{V_E}, \quad (3)$$

where  $P_E$  and  $P_p$  are the initial and product pressures, respectively;  $V_E$  and  $V_p$  are the initial specific volume and product specific volume of the explosives, respectively;  $C_v$  is the heat capacity;  $T_0$  is the initial temperature of the explosive;  $T_p$  is the product temperature; and  $A$ ,  $B$ ,  $R_1$ ,  $R_2$ , and  $\omega$  are constants.

The jet-initiating covered explosive was simulated using literature values [23] for the ignition-and-growth model parameters of the RDX-based aluminized explosive. The accuracy of the simulation results was verified by comparing them with the experimental results. We calculated the jet initiation at different explosive temperatures for different cover thicknesses. Furthermore, we obtained the law relating the cover-thickness threshold to temperature and studied the effect of this law on the detonation-wave growth of the RDX-based aluminized explosive for both impact and bow-wave initiation.

## 4 Results and Discussion

### 4.1 Characteristics of Shaped-Charge Jet

Figure 4 compares the radiographed and simulated shaped-charge jet and tip position at different times. The jet formation can be observed via jet shapes at different times. At 6.5  $\mu\text{s}$ , the jet began to form. At 7  $\mu\text{s}$ , the jet tip reached 3 mm away from the shaped-charge, and the jet length was 28.55 mm. By 10  $\mu\text{s}$ , the jet has reached a distance of 23 mm, and the jet length has increased to 47.85 mm. At 12  $\mu\text{s}$ , the jet has increased to 61.2 mm. The jet tip has flown 37 mm. The jet was in a progressive state before 14  $\mu\text{s}$  and developed into a stable shape after this time. The simulated and experimental jet shapes were consistent at 14  $\mu\text{s}$  and 15  $\mu\text{s}$ . The calculated jet lengths were 71.96 mm and 81.45 mm and the experimental lengths were 74.81 mm and 77.79 mm at these respective times. The rel-

**Table 1.** Parameters of JWL equation of state of explosive products.

Explosive	$\rho_0(\text{g}/\text{cm}^3)$	$P_C(\text{GPa})$	$D(\text{m}/\text{s})$	$E_0(\text{MJ}/\text{m}^3)$
HMX-based	1.82	37	8800	0.102
A(GPa)	B(GPa)	R <sub>1</sub>	R <sub>2</sub>	$\omega$
4.6	0.1802	4.6	1.3	0.38

**Table 2.** Parameters of material model.

Material	$\rho$ ( $\text{g}/\text{cm}^3$ )	$G_0$ (GPa)	$\sigma_0$ (GPa)	$C$ ( $\text{m}/\text{s}$ )	$s$	$\gamma_0$	$a$
steel	7.83	67	1.85	4569	1.49	2.17	0
copper	8.96	47.7	–	3940	1.49	1.99	0

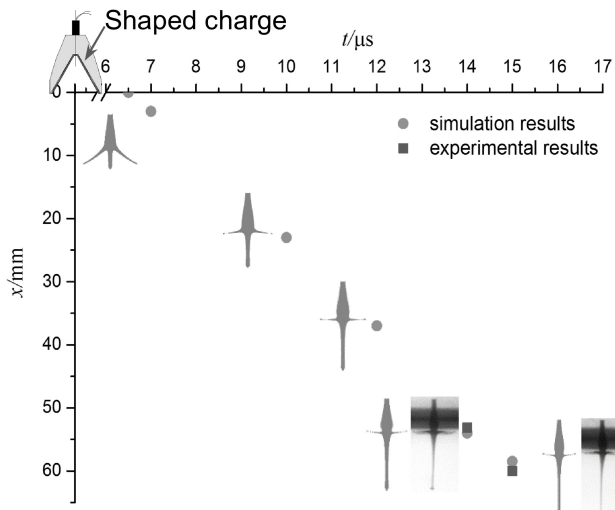


**Figure 4.** Comparison of radiographed and simulated shaped-charge jet and tip position at different times.

ative error was within 5%. The jet-penetration speed was calculated by measuring the jet tip position at different times. The calculated jet velocity was  $\sim 7000$  m/s, the experimental speed was  $\sim 6892$  m/s, and the relative error was 1.57%. The measured jet diameter was 2.19 mm, and the calculated diameter was 2 mm with an error of 9.5%. Therefore, the calculation describes shaped-charge jet-formation effectively.

#### 4.2 Jet-Initiation Characteristics of Explosive for Covers of Different Thicknesses

Figure 5 shows X-ray radiographs of the shaped-charge jet and explosive at  $25^\circ\text{C}$  for a 2-mm-thick cover. The jet penetrated the explosive to a depth of 5.83 mm in the X-ray ra-

diograph at  $18.65 \mu\text{s}$ , and a spherical detonation wave formed around the jet tip inside the explosive. The detonation wave-front was at a depth of 15.06 mm from the upper surface of the explosive charge, as shown in Figure 5(a). At  $19.65 \mu\text{s}$ , the detonation wave continued to propagate downward and developed into a surface detonation wave because of the effect of the side rarefaction wave. The distance between the detonation wave-front and the jet tip was 11.66 mm. The detonation wave was faster than the jet tip, as shown in Figure 5(b). Figure 6 shows the calculated pressure distribution along the central axis of the longitudinal section of the explosive at different times for the 2-mm cover at  $25^\circ\text{C}$ . Detonation-wave growth can be seen from the graphs. At  $15.95 \mu\text{s}$ , the jet tip had just entered the explosive and the pressure reached 20 GPa at 0.7 mm in front of the jet tip, which indicates that the explosive had been initiated and a detonation wave generated. The spherical detonation wave continued to propagate downward. At  $17.34 \mu\text{s}$ , the pressure decreased to 16.6 GPa and the distance between the detonation wave-front and jet tip increased to 2.75 mm. At  $18.65 \mu\text{s}$ , the spherical detonation wave expanded further and was about to reach the side of the charge. The detonation wave shape was consistent with that observed experimentally. The calculated detonation wave position was 2.19 mm ahead of the experimental position, and the relative error was small. The maximum pressure was 20.3 GPa. At  $19.65 \mu\text{s}$ , the detonation wave had propagated to the side of the explosive, which was consistent with the experiment. The pressure reached 21.8 GPa, which suggests that the detonation wave was stable.

Figure 7 shows X-ray radiographs of the shaped-charge jet and explosive at  $25^\circ\text{C}$  for a 27-mm-thick cover. The X-ray radiograph at  $26.95 \mu\text{s}$  shows that the jet penetrated the explosive at a depth of 15.63 mm. The detonation wave formed ahead of the jet tip at 19.54 mm from the upper surface of the charge, as shown in Figure 7(a). At  $28.95 \mu\text{s}$ , the detonation wave continued to propagate forward and a

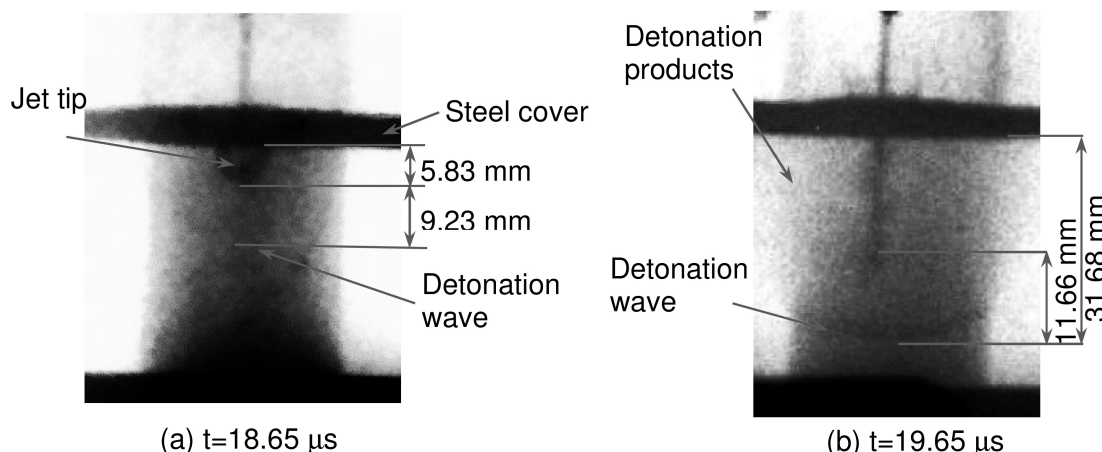


**Figure 5.** X-ray radiographs of a shaped-charge jet and explosive at  $25^\circ\text{C}$  for a 2-mm thick cover

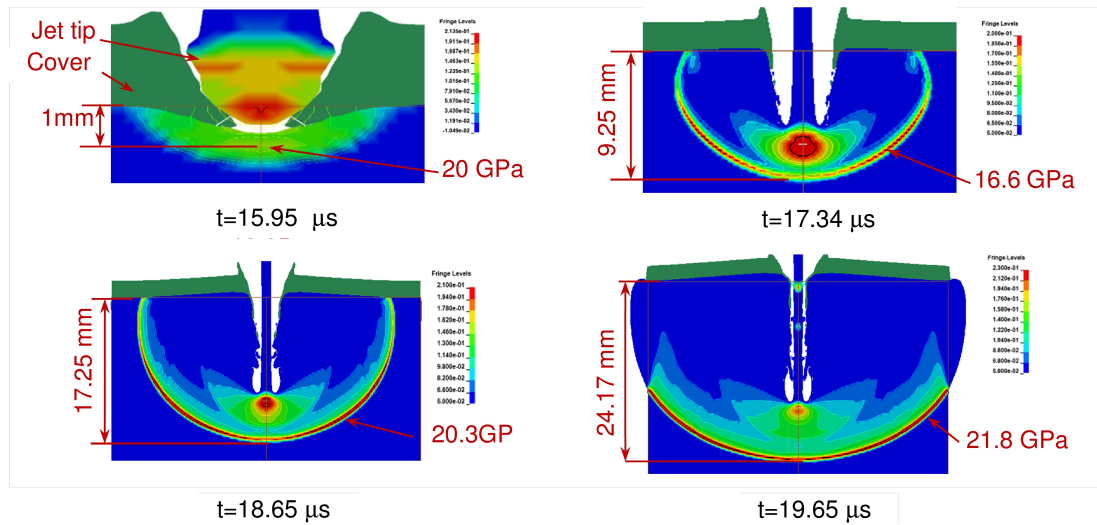


**Figure 6.** Calculated pressure distribution along the central axis of the longitudinal section of the explosive at different times for a 2-mm steel cover at 25°C.

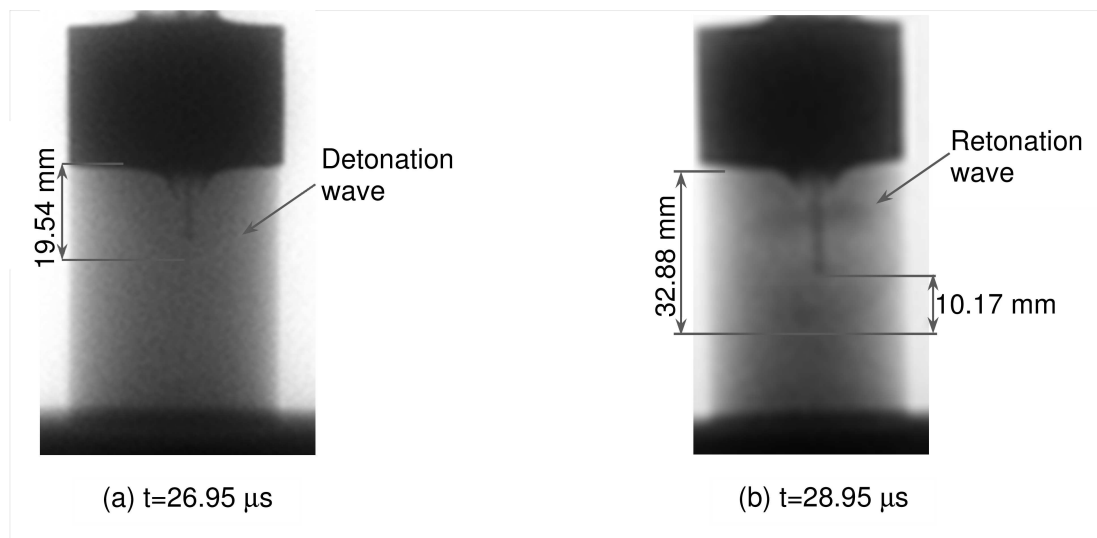


**Figure 7.** X-ray radiographs of a shaped-charge jet and explosive at 25 °C for a 27-mm-thick cover.

retonation wave appeared above the jet tip, which moved back to the upper surface of the charge. The distance between the jet tip and the detonation wave was 10.17 mm, and the detonation wave was significantly faster than the jet tip, as shown in Figure 7(b). Figure 8 shows the calculated pressure distribution along the central axis of the longitudinal section of the explosive at different times for the 27-mm-thick cover at 25 °C. The detonation-wave growth is visible in the graphs. At 26.0  $\mu\text{s}$ , the jet tip penetrated the explosive at a depth of 5.75 mm, and the explosive pressure close to the jet tip reached 12.6 GPa. The pressure along the central axis of the longitudinal section of the explosive decreased gradually with increasing explosive-charge depth. There was a minimum pressure of 6 GPa, 3 mm from

the jet tip. A pressure of 9.44 GPa was reached at a depth of 4.45 mm from the tip, showing that the explosive was initiated here and an initiation region had formed. At 26.1  $\mu\text{s}$ , when the jet tip penetrated the explosive to a depth of 6.25 mm, a curved detonation wave was formed ~3.25 mm in front of the jet tip. The maximum detonation-wave pressure was 10.9 GPa, which was lower than that under steady detonation. At 26.95  $\mu\text{s}$ , the bow wave continued to expand further; it propagated downward and moved back to the upper explosive surface, and the retonation wave formed. The calculated detonation wave propagated to an explosive depth of 15.2 mm, which was almost the same as the experimentally observed position. The maximum explosive pressure was 20.8 GPa. The detonation wave propagated to

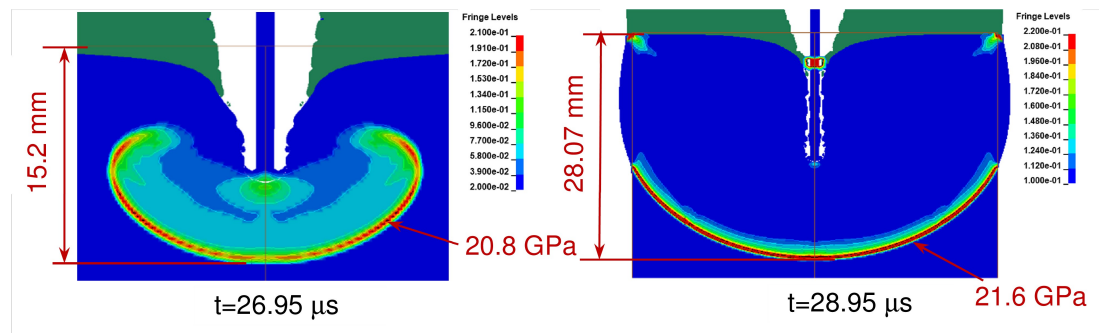


**Figure 8.** Calculated pressure distribution along the central axis of the longitudinal section of the explosive at different times for a 27-mm-thick cover at 25°C.

the side of the explosive and the maximum pressure reached 21.6 GPa at 28.95 μs, at which point the detonation wave reached a stable propagation state.

Figure 9 shows the calculated pressure distribution along the central axis of the explosive at different times for a 27-mm-thick cover at 25°C. The jet-initiation characteristics can be obtained from the pressure variation with depth in Figure 9. At 26.0 μs, the pressure was 10 GPa at a depth of 5.75 mm, which was the jet-tip pressure. At 6 mm, the explosive pressure increased to 12.6 GPa. Then, the pressure decreased gradually to 6 GPa with increasing explosive depth. Finally, the pressure increased to 9.44 GPa at 9 mm, followed by an immediate drop to 0, which indicates that the explosive was initiated at 9 mm. These results are consistent with the bow-wave-initiation characteristics described by Chick et al [7,8]. Therefore, a bow wave formed at a depth of 9 mm. When the tip pressure at a depth of 9 mm was ~10 GPa at 26.95 μs, the explosive pressure in front of the jet tip increased to ~13 GPa, and the pressure decreased gradually. The pressure was 6 GPa until a depth of 11 mm, which was the same tendency as in the pressure

distribution at 26.0 μs. The pressure increased slowly at a depth of 14 mm. However, the pressure increased to 21 GPa abruptly at ~14.5 mm, which indicates that the detonation reaction had occurred. The shock wave generated by the jet tip caught up with the former shock wave-front and provided energy to support the explosive detonation, which is an important condition for bow-wave formation. Therefore, we conclude from the calculated pressure distribution along the central axis of the explosive at different times that the initiation for a 27-mm-thick cover at 25°C was due to a bow wave.

These results show that the shaped-charge jet penetrated the thin cover to initiate an explosively high pressure on the upper surface of the charge when the jet contacted the explosive. Therefore, the explosive was detonated in a short time with a short run-to-detonation distance. When the jet penetrated the thick cover, the explosive was initiated at a certain distance from the jet tip inside the explosive, which caused a relatively long run-to-detonation distance. A retonation wave appeared, belonging to the bow-wave initiation mechanism.

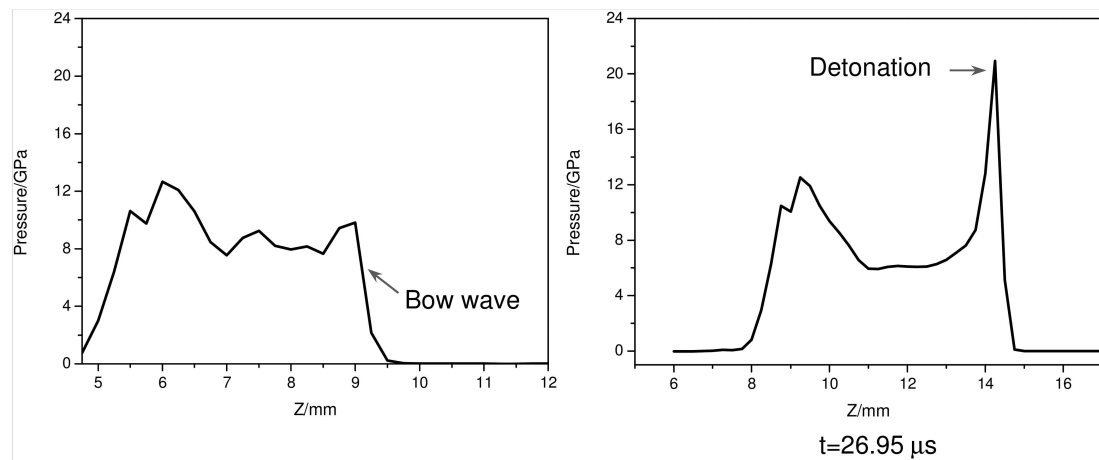
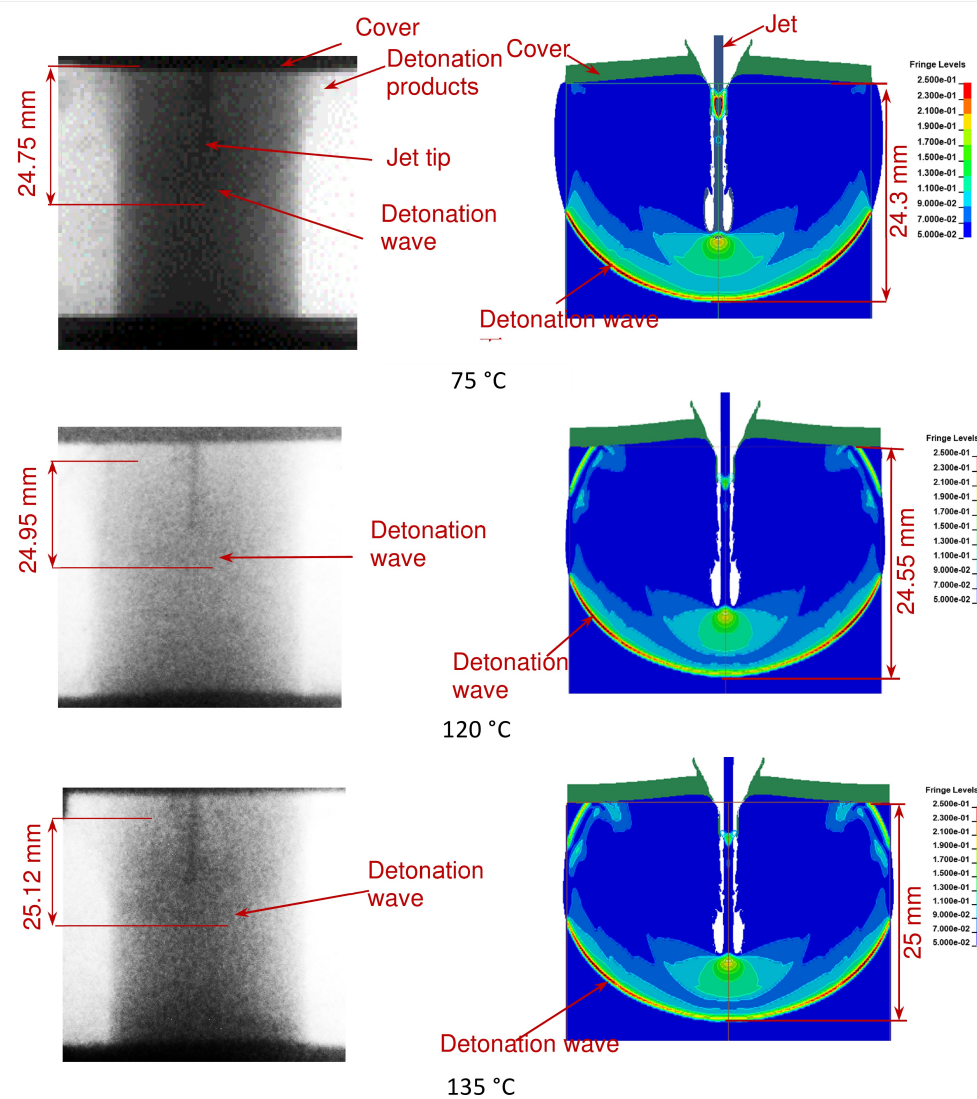


**Figure 9.** Calculated pressure distribution along the central axis of the explosive at different times for a 27-mm-thick cover at 25°C.

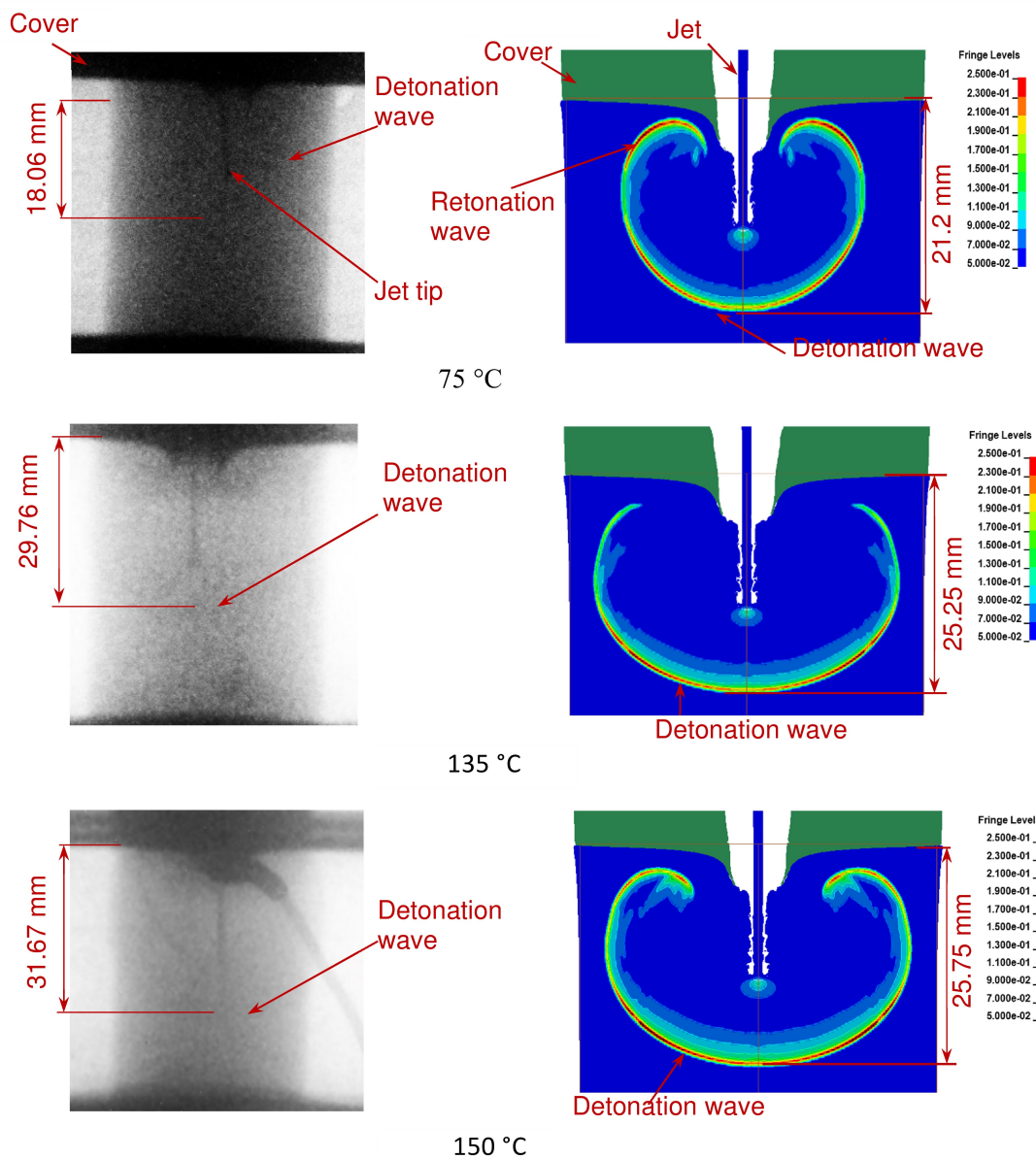
## 4.3 Jet-Initiation Characteristics of Explosive at Different Temperatures for Covers of Different Thicknesses

Figure 10 shows the jet and explosive X-ray radiographs and calculated pressure distribution along the central axis of the longitudinal section for different explosive temperatures with a 2-mm thick cover at 19.65  $\mu$ s. The detonation-wave propagation characteristics were almost the same as those at 25 °C belonging to prompt impact initiation under a thin cover. However, the detonation-wave propagation distance of the explosive at 75 °C was shorter than at 25 °C, indicating reduced shock sensitivity, and the detonation-wave propagation distances at 120 °C and 75 °C were not much different. The detonation-wave propagation distance at 135 °C was longer than at 120 °C, which shows that the shock sensitivity at 135 °C increased compared with that at

120 °C. Figure 11 shows the jet and explosive X-ray radiographs and calculated pressure distribution along the central axis of the longitudinal section for different explosive temperatures for a 27-mm-thick cover at 28.95  $\mu$ s. There was a retonation wave, and the detonation-wave propagation characteristics were almost the same as at 25 °C. However, the detonation-wave propagation distance was 14.82 mm shorter at 75 °C than at 25 °C, which suggests that the shock sensitivity of the explosive at 75 °C was lower than that at 25 °C. The detonation-wave propagation distance increased at 135 °C, indicating increased shock sensitivity of the explosive at 135 °C. The detonation-wave propagation distance at 150 °C was longer than that at 135 °C, showing that the shock sensitivity of the explosive increased with increasing temperature.



**Figure 10.** Jet and explosive X-ray radiographs and calculated pressure distribution along the central axis of the longitudinal section for different explosive temperatures for a 2-mm-thick cover at 19.65  $\mu$ s.



**Figure 11.** Jet and explosive X-ray radiographs and calculated pressure distribution along the central axis of the longitudinal section for different explosive temperatures for a 27-mm-thick cover at 28.95  $\mu$ s.

#### 4.4 Effect of Explosive Temperature and Cover Thickness on Detonation-Wave Growth

Many simulations were carried out for jet-initiating explosives with different cover thicknesses and temperatures using the relationship between  $G_1$  and temperature in the ignition-and-growth model. Figure 12 shows the calculated critical cover thicknesses at different explosive temperatures and their fitted linear relationship for both impact and bow-wave initiation. The cover-thickness boundary that separates impact initiation and bow wave initiation decreased linearly as temperature increased from 25 °C to 111 °C. However, the cover-thickness boundary increased as

temperature increased from 111 °C to 170 °C. Equation (5) shows the linear relationship obtained via piecewise fitting. For bow-wave initiation in the range of 25–111 °C, the cover-thickness threshold decreased linearly with increasing temperature. For 111–170 °C, the thickness threshold increased as the temperature continued to increase. Equation (6) shows the linear relationship obtained via piecewise fitting.

The relationship between the cover-thickness boundary that separates impact initiation and bow wave initiation and explosive temperature is

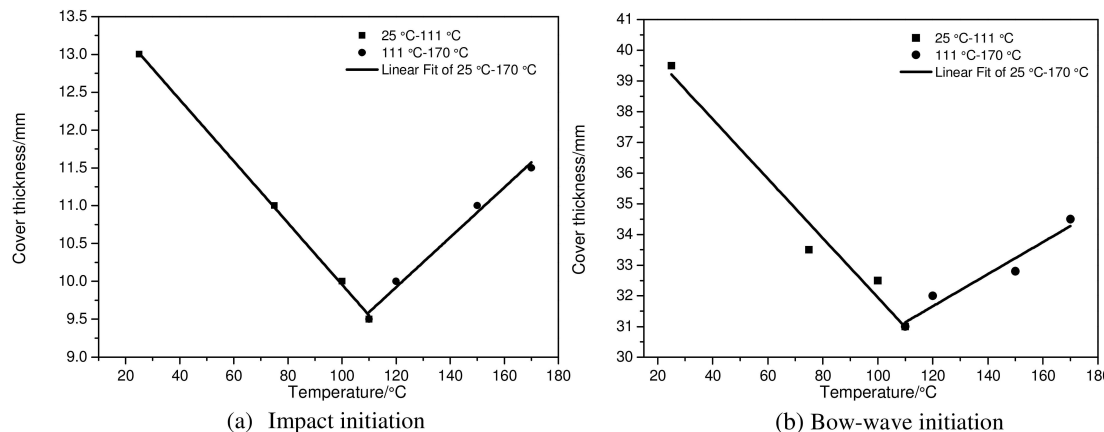


**Figure 12.** Cover-thickness threshold of different explosive temperatures and fitted linear relationships for impact and bow-wave initiation.

$$d_1 = \begin{cases} 14.003 - 0.041T & 25^\circ\text{C} \leq T \leq 111^\circ\text{C} \\ 5.96 + 0.03T & 111^\circ\text{C} < T \leq 170^\circ\text{C} \end{cases}. \quad (5)$$

The relationship between the cover-thickness threshold and explosive temperature for bow-wave initiation is

$$d_2 = \begin{cases} 41.629 - 0.09T & 25^\circ\text{C} \leq T \leq 111^\circ\text{C} \\ 25.3978 + 0.052T & 111^\circ\text{C} < T \leq 170^\circ\text{C} \end{cases}. \quad (6)$$

In Eqs. (5) and (6),  $d_1$  and  $d_2$  are the cover thicknesses in mm, and  $T$  is the temperature in °C.

These two equations can be used to analyze the safeties of the jets that initiated explosions at different temperatures for different cover thicknesses.

The pressure generated inside the explosive was much greater than the critical initial pressure under jet-impact initiation. Therefore, the jet-initiating sensitivity of the covered explosive was determined mainly by the bow-wave characteristics. The run-to-detonation distance reflects the shock sensitivity of the explosive under certain conditions. Figure 13 shows the run-to-detonation distance calculated for different explosive temperatures with covers of different thicknesses for bow-wave initiation. The distance increases as the cover thickness increases at constant temperature, indicating gradual reduction of the shock sensitivity of the explosive. Therefore, one can predict the jet-initiation sensitivity of the explosive at different temperatures under different cover thicknesses.

## 5 Conclusion

We established a practical method for accurately controlling the temperature of a heated explosive under a jet-initiating cover. Jet-initiation tests were performed on a heated explosive. X-ray photography was used to obtain the

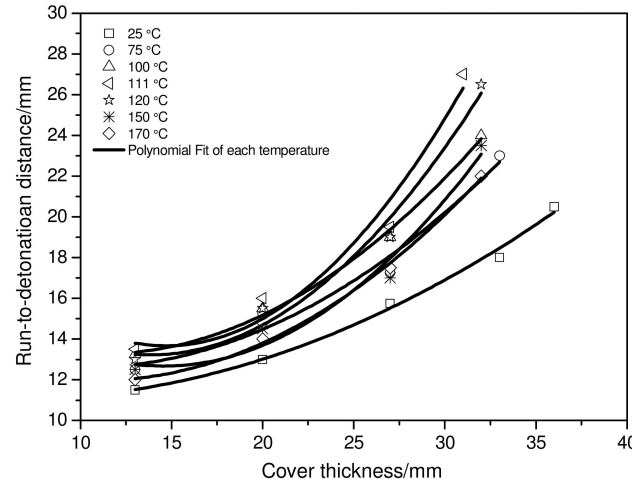


**Figure 13.** Run-to-detonation distance of different explosive temperatures covered by different thicknesses in bow-wave initiation.

detonation-wave shape and propagation characteristics in the jet-initiating heated explosive. Prompt impact initiation occurred with a thin cover, and the explosion was initiated near the upper surface of the explosive. However, the explosion under a thick cover was initiated by a bow wave generated at a certain distance from the surface of the explosive, and a retonation wave was observed.

The temperature of the RDX-based aluminized explosive significantly affected the shock sensitivity. For a certain temperature range, the shock sensitivity of the explosive to the jet decreased as the temperature increased; however, above a certain temperature, the shock sensitivity increased with increasing temperature. We established a method of simulating the main parameters as piecewise functions of temperature in each initiation model. Predictions can be calculated for the jet-initiating explosive at different heated temperatures. Calculating the run distance to detonation during jet initiation at different explosive temperatures un-

der covers of varying thicknesses provides a basis for safety analysis and evaluation of warheads.

## Acknowledgements

This work was supported by the National Natural Science Foundation of China [grant number 11832006] and the project of State Key Laboratory of Explosion and Science (Beijing Institute of Technology), the opening project number is KFJJ18-02 M.

## References

- [1] *The Initiation of an Exploder by a Munroe Jet (Flash Radiography)*, Armament Research Department, Apr. ARD Met. Report 45, 1945.
- [2] L. Zernow, I. Lieberman, S. Kronman, *An Exploratory Study of the Initiation of Steel-Shielded Composition B by Shaped Charge Jets*. Ballistic Research Laboratories, BRL Memo Report 944, Oct 1955.
- [3] M. Held, Initiation of Explosives, a multiple Problem of the physical of Detonation, *Explosivstoffe* 1968, 5, 98–113.
- [4] C. L. Mader, G. H. Pimbley, *Jet Initiation of Explosives*, LA Report 8647, Feb. 1981.
- [5] C. L. Mader, G. H. Pimbley, Jet Initiation and Penetration of Explosives, *J. Energ. Mater.* 1983, 1, 3–44.
- [6] M. C. Chick, D. J. Hatt, The Initiation of Covered Composition B by a Metal Jet, *Propellants Explos. Pyrotech.* 1983, 8, 121–126.
- [7] M. C. Chick, I. R. Macintyre, R. B. Frey. The Jet Initiation of Solid Explosives, *The 8th International Symposium on Detonation Preprints*, Lawrence Livermore National Laboratory, CA, 1985, p. 20.
- [8] M. C. Chick, T. J. Bussell, R. B. Frey, A. Bines, Jet Initiation Mechanisms and Sensitivities of Covered Explosives. *Proceedings of the 9th International Symposium on Detonation*, Portland, OR, 1989.
- [9] R. Frey, W. Lawrence, M. Chick, Shock Evolution After Shaped Charge Jet Impact and Its Relevance to Explosive Initiation, *Internat. J. Impact Eng.* 1995, 16, 563–570.
- [10] M. C. Chick, T. J. Bussell, The Effect of Minimum Detonation Diameter on the Mechanism of Jet Initiation of Bare Explosives, *J. Appl. Phys.* 1988, 63, 4761–4763.
- [11] W. Lawrence, J. Starkenberg, The Effects of the Failure Diameter of an Explosive on Its Response to Shaped Charge Jet Attack, *Internat. J. Impact Eng.* 1997, 20, 499–510.
- [12] M. C. Chick, T. J. Bussell, R. B. Frey, Some Characteristics of Bow Wave Initiation and Desensitization. *The 10th Symposium (International) on Detonation*, Boston, 1993.
- [13] C. Mellor, H. R. James, M. J. Goff, A Theoretical Exploration of the Differences between Prompt and Bow Shock Initiation of Explosives by Shaped Charge Jets, *17th Conference of the American Physical Society Topical Group on Shock Compression of Condensed Matter*, Chicago, Illinois (USA), June 26 – July 1, 2011, AIP Conference proceedings 1426, p. 287, <https://doi.org/10.1063/1.3686275>.
- [14] H. R. James, C. Mellor, M. J. Goff, The Effect of Failure Diameter on the Initiation of Explosives by Shaped Charge Jet, *17th Conference of the American Physical Society Topical Group on Shock Compression of Condensed Matter*, Chicago, Illinois (USA), June 26 – July 1, 2011, AIP Conference proceedings 1426, p. 291, <https://doi.org/10.1063/1.3686276>.
- [15] W. Arnolda, E. Rottenkolber, High Explosive Initiation Behavior by Shaped Charge Jet Impacts, *Procedia Eng.* 2013, 58, 184–193, <https://doi.org/10.1016/j.proeng.2013.05.022>.
- [16] M. Held, Jet Initiation of Covered High Explosives with Different Materials, *Propellants Explos. Pyrotech.* 2002, 27.
- [17] H. R. James, The Role of Tip Geometry in the Initiation of Explosives by Shaped Charge Jet, *13th Conference of the American Physical Society Topical Group on Shock Compression of Condensed Matter*, Portland, Oregon (USA), July 20 – 25, 2003, AIP Conference Proceedings 706, p. 993 .
- [18] A. C. Schwartz, *Flyer Plate Performance and Initiation of Insensitive Explosives by Flyer Plate Impact*, SAND-75-20461, 1975.
- [19] P. A. Urtiew, J. W. Forbes, C. M. Tarver, K. S. Vandersall, F. Garcia, D. W. Greenwood, P. C. Hsu, J. L. Maienschein, Shock Sensitivity of LX-04 Containing Delta Phase HMX at Elevated Temperatures, *13th Conference of the American Physical Society Topical Group on Shock Compression of Condensed Matter*, Portland, Oregon (USA), July 20 – 25, 2003, AIP Conference Proceedings 706, p. 1053.
- [20] F. Garcia, K. S. Vandersall, C. M. Tarver, P. A. Urtiew, Shock Initiation Experiments on the LLM-105 Explosive RX-55-AA at 25 °C and 150 °C with Ignition and Growth Modeling, *15th APS Topical Conference on Shock Compression of Condensed Matter*, Kohala Coast, Hawaii, USA, June 24–29, 2007, AIP Conference Proceedings 955, p. 907.
- [21] R. L. Gustavsen, R. J. Gehr, S. M. Bucholtz, R. R. Alcon, B. D. Bartram, Shock Initiation of the Tri-amino-tri-nitro-benzene Based Explosive PBX 9502 Cooled to -55 °C, *J. Appl. Phys.* 2012, 112, 114907 ~ 1248.
- [22] R. L. Gustavsen, R. J. Gehr, S. M. Bucholtz, A. H. Pacheco, B. D. Bartram, Shock initiation of the TATB Based Explosive PBX 9502 Heated to ~76 °C, *19th Conference of the American Physical Society Topical Group on Shock Compression of Condensed Matter*, Tampa, Florida (USA), June 14 – 19, 2015, AIP Conference proceedings 1793, 030017.
- [23] R. L. Gustavsen, B. D. Bartram, L. L. Gibson, A. H. Pacheco, J. D. Jones, A. B. Goodbody, Shock Initiation of TATB Based Explosive PBX 9502 heated to 130 °C, *20th Biennial Conference of the APS Topical Group on Shock Compression of Condensed Matter*, St. Louis, Missouri, USA, July 9–14, 2017, AIP Conference Proceedings 1793, p.100015.
- [24] Z. Pi, L. Chen, J. Wu, Temperature-dependent Shock Initiation of CL-20 based High Explosives, *Cent. Eur. J. Energ. Mat.* 2017, 14, 361 ~ 374.
- [25] P. Zhao, L. Chen, K. Yang, D. S. Geng, J. Y. Lu, J. Y. Wu, Effect of Temperature on Shock Initiation of RDX-Based Aluminized Explosives, *Propellants Explos. Pyrotech.* 2019, 44, 1562–1569.
- [26] Z. Pi, L. Chen, Q. Liu, J. Y. Wu, Shock initiation of CL-20 based explosives, *Explosion, And Shock Waves.* 2017, 37, 915–923.
- [27] J. O. Hallquist, *LS-DYNA keyword user's manual*, Livermore Software Technology Corporation, 2007.
- [28] C. M. Tarver, J. O. Hallquist, L. M. Erickson. Modeling Short Pulse Duration Shock Initiation of Solid Explosives, *Proceedings of the 8th International Symposium of Detonation*. Albuquerque, USA, 1985, 951–961.

Manuscript received: September 11, 2019  
Version of record online: July 16, 2020